

SWORD M-SCH-B2735 - P-RICH IRON - IRON AGE - SWITZERLAND

Artefact name Sword M-Sch-B2735

Authors Marianne. Senn (Empa, Dübendorf, Zurich, Switzerland) & Christian. Degrigny (HE-Arc CR, Neuchâtel, Neuchâtel, Switzerland)

Url /artefacts/1441/

▼ The object



Fig. 1: Sword (after Senn Bischofberger 2005, 241).

Credit HE-Arc CR.

▼ Description and visual observation

Description of the artefact Sword of the middle La Tène type, broken into two parts (Fig. 1). Under a hand lens the surface shows parallel grinding traces from mechanical cleaning.

Type of artefact Weapon

Origin Marin-Epagnier, La Tène, Saint-Blaise, Neuchâtel, Switzerland

Recovering date Water finds, end 19th/beginning 20th cent. AD

Chronology category Iron Age

chronology tpp 250 B.C. ▾

chronology taq 140 B.C. ▾

Chronology comment La Tène C

Burial conditions / environment Soil

Artefact location Museum Schwab, Biel/Bienne, Bern

Owner Museum Schwab, Biel/Bienne, Bern

Inv. number M-Sch-B2735

Recorded conservation data Conserved (not recorded, but mechanical cleaning visible)

Complementary information

None.

▼ Study area(s)



Fig. 2: Location of sampling area,

Credit HE-Arc CR.

▼ Binocular observation and representation of the corrosion structure

None.

▼ MiCorr stratigraphy(ies) – Bi

▼ Sample(s)

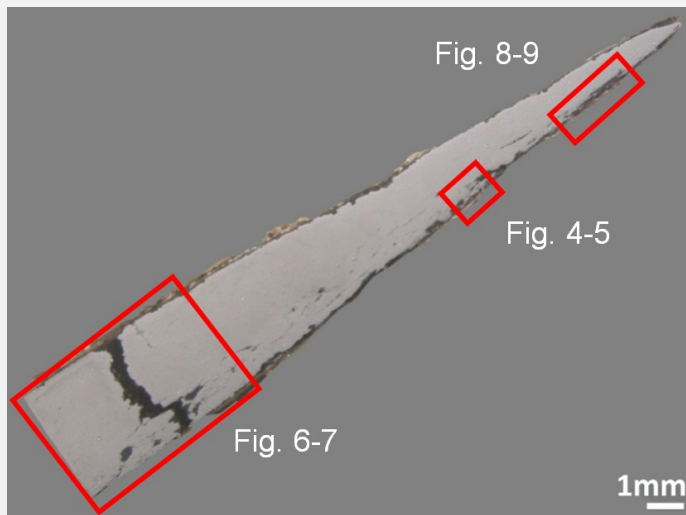


Fig. 3: Micrograph of the cross-section of the sample taken from the sword showing the location of Figs. 4 to 9,

Credit HE-Arc CR.

Description of sample

The sample includes half of the sword blade (Figs. 2 and 3). The corrosion layer is thin (Fig. 3).

Alloy

P-rich iron

Technology

Forged, annealed and cold worked

Lab number of sample

M-SCH-B2735

Sample location

HE-Arc CR, Neuchâtel, Neuchâtel

Responsible institution

Schweizerisches Landesmuseum, Zürich, Zurich

Date and aim of sampling

1969, metallography

Complementary information

None.

▼ Analyses and results

Analyses performed:

Metallography (nital etched), Vickers hardness testing, LA-ICP-MS, SEM/EDS.

▼ Non invasive analysis

None.

▼ Metal

The remaining metal is a P-rich (0.2 mass%) iron (Table 1) with long parallel slag inclusions (Fig. 4) concentrated on one side of the blade. The slag inclusions are composed of wüstite/FeO dendrites and fayalite/Fe₂SiO₄ in a glassy matrix (Fig. 5 and Table 2). Their chemical composition is typical for iron produced by the bloomery process (dominated by iron oxides and silica). It is difficult to identify the ore type from the slag composition. Interestingly in one case the slag composition is very specific (alumina and P-rich material). After etching, the metal shows a ferritic structure (Fig. 6). The grain size is variable (between ASTM grain sizes of 4 to 7) and some grains include Neuman bands (Fig. 7). A large crack has developed through the metal section (Figs. 3 and 6). The average hardness of the metal (HV1 185) is quite high for a wrought iron. The level of hardness and Neuman bands are typical for a P-rich iron. Neuman bands are said to develop by cold working and shock deformation. According to Swiss and McDonnell 2003 they form when little cold work is carried out. Distortion (grain deformation) after cold working starts to be apparent in iron after a reduction in thickness of between 30-40%. Since no grain deformation is visible, the present reduction is probably a little less than this range.

| Elements | V | Cr | Mn | P | Co | Ni | Cu | As | Ag |
|-----------------------|---|----|----|------|-----|-----|-----|-----|-----|
| Median mg/kg | < | 5 | 10 | 2200 | 140 | 270 | 500 | 260 | < |
| Detection limit mg/kg | 1 | 4 | 1 | 50 | 1 | 1 | 1 | 2 | 0.1 |
| RSD % | - | 56 | 48 | 10 | 14 | 16 | 37 | 15 | - |

Table 1: Chemical composition of the metal (<: below the detection limit). Method of analysis: LA-ICP-MS, Lab Analytical Chemistry, Empa (for details see Devos et al. 2000).

| Structure | MgO | Al ₂ O ₃ | SiO ₂ | P ₂ O ₅ | K ₂ O | CaO | TiO ₂ | MnO | FeO | Total | SiO ₂ /Al ₂ O ₃ |
|-------------------------------|-----|--------------------------------|------------------|-------------------------------|------------------|-----|------------------|-----|-----|-------|--|
| Wüstite in glass | <1 | 2 | 15 | 3 | < | <1 | < | < | 87 | 108 | Around 8 |
| Wüstite and fayalite in glass | < | 5 | 24 | <1 | 1 | 1 | < | < | 70 | 103 | Around 5 |
| Wüstite and fayalite in glass | <1 | 3 | 23 | 2 | < | 1 | < | < | 69 | 98 | Around 8 |
| Fayalite in glass | < | 6 | 26 | 3 | 1 | 1 | < | < | 72 | 109 | Around 5 |
| Fayalite phase | 1 | 1 | 31 | 1 | <1 | 1 | < | 1 | 69 | 106 | Around 31 |
| Fayalite in glass | < | 9 | 24 | 3 | 1 | 1 | <1 | < | 66 | 105 | Around 3 |

Table 2: Chemical composition of the slag inclusions (mass%, <: below the detection limit) at the tip (pearlite) and the body (ferrite) of the knife. Method of analysis: SEM/EDS, Laboratory of Analytical Chemistry, Empa.

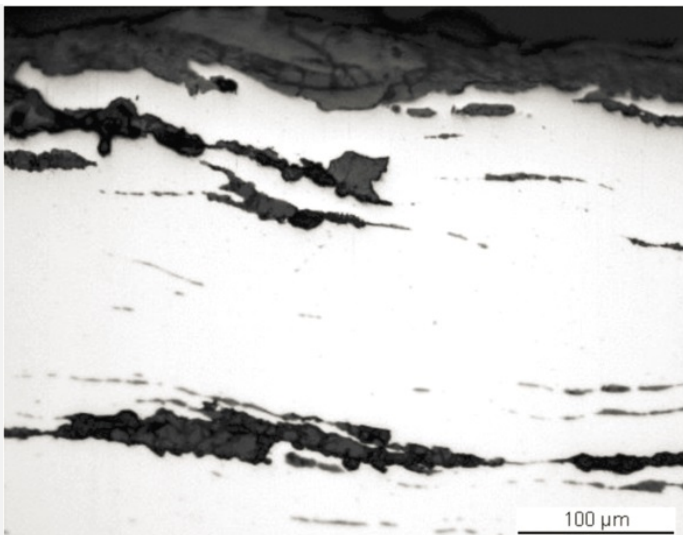


Fig. 4: Micrograph of the metal sample from Fig. 3 (detail, rotated by 225°), unetched, bright field. In white the metal containing elongated slag inclusions (in grey); in black porosity.

Credit HE-Arc CR.

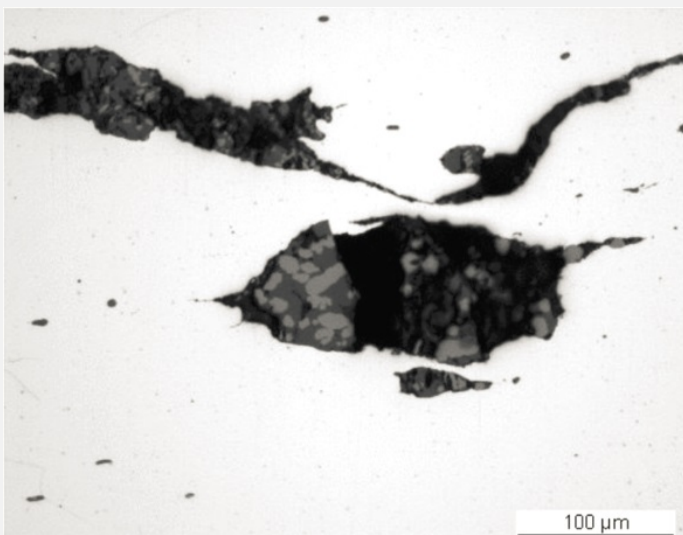


Fig. 5: Micrograph of the metal sample from Fig. 3 (detail), unetched, bright field. Detail with slag inclusions showing a structure with wüstite dendrite (light-grey) and fayalite (dark-grey),

Credit HE-Arc CR.

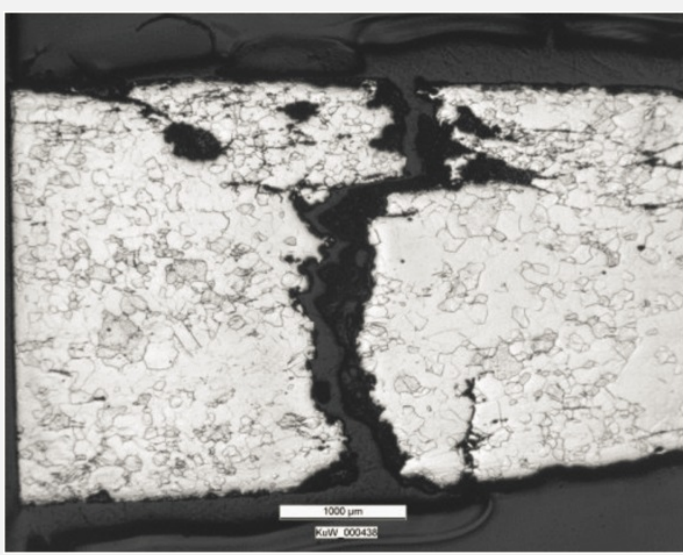


Fig. 6: Micrograph of the metal sample from Fig. 3 (reversed picture, rotated by 225°, detail), etched, bright field. Metal with a large pre-existing crack and ferritic, recrystallized structure. Grains have different sizes,

Credit HE-Arc CR.

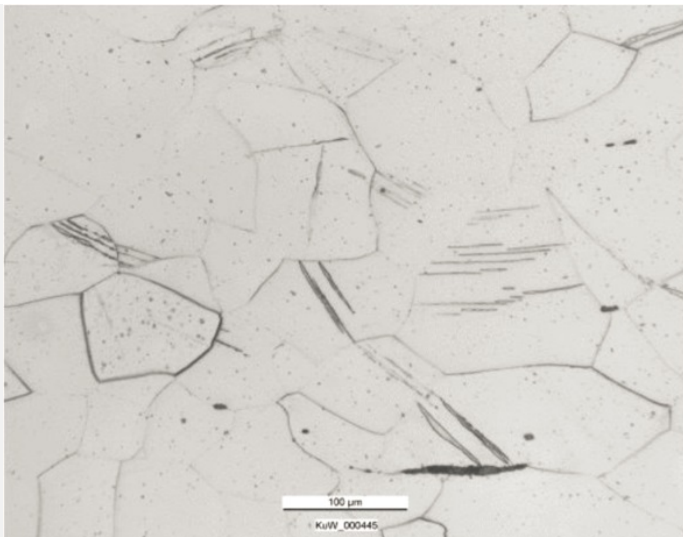


Fig. 7: Micrograph of the metal sample (detail of Fig. 6), etched, bright field. Ferrite grains including Neuman bands formed after cold working in a P-rich iron,

Credit HE-Arc CR.

Microstructure Recrystallized grains, Newman bands, ghost structure

First metal element Fe

Other metal elements P

Complementary information

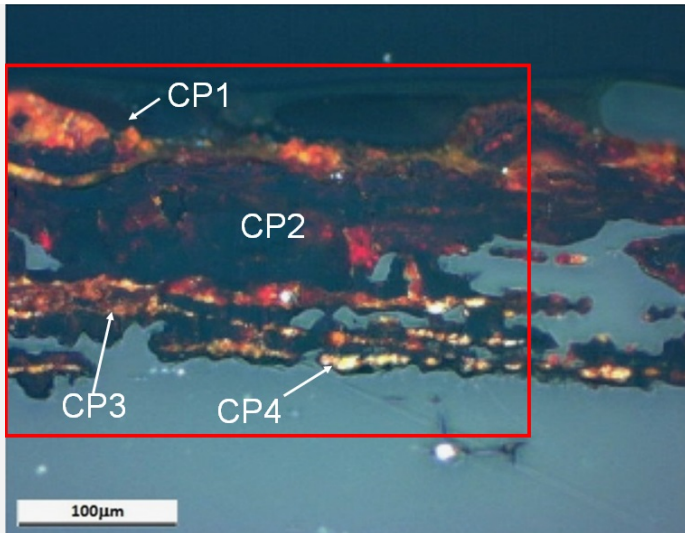
None.

▼ Corrosion layers

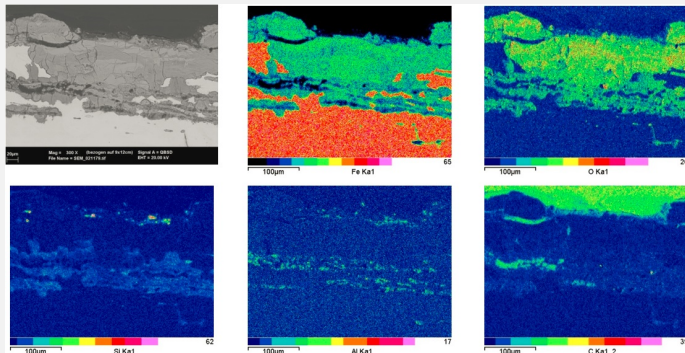
The remaining metal, including the large crack, is covered by a thin, fissured corrosion crust (Figs. 3, 4, 6 and 8). The corrosion crust is thicker on the side containing the long slag inclusions (Fig. 3). In bright field and in the BSE-mode of the SEM image only light and dark-grey areas can be distinguished (Figs. 4 and 9). Under polarised light the corrosion products appear yellow-orange near the metal surface and then become successively dark-red and black. The outer layer (CP1) is orange-yellow, as is the inner one (CP4, Fig. 8). There is a correlation between the level of grey in SEM/BSE-mode, the colours under polarised light, and the chemical composition of the corrosion layer (Table 3, Figs. 8 and 9). The lighter the grey of the SEM/BSE-mode, or the colours (light-brown and red) under polarised light, the richer the area is in Fe and the more depleted it is in O. Surprisingly the inner corrosion layers (CP3 and CP4) are contaminated with Si, Al and O.

| Elements | O | Si | Fe | Total |
|--|----|----|----|-------|
| Light or dark-red corrosion products (CP3) | 25 | 2 | 67 | 94 |
| Light or dark-red corrosion products (CP3) | 32 | < | 74 | 108 |
| Dark or dark-red corrosion products (CP2) | 41 | < | 67 | 109 |

Table 3: Chemical composition (mass %, <: below the detection limit) of the corrosion layer (from Fig. 9). Method of analysis: SEM/EDS, Laboratory of Analytical Chemistry, Empa.



Credit HE-Arc CR.



Credit HE-Arc CR.

| | |
|----------------|-------------------------|
| Corrosion form | Uniform - transgranular |
| Corrosion type | Unknown |

Complementary information

None.

▼ MiCorr stratigraphy(ies) – CS

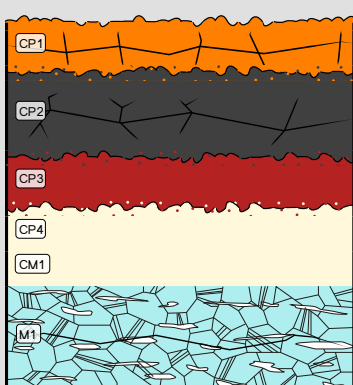


Fig. 8: Micrograph showing the metal - corrosion crust interface from Fig. 3 (inverted picture, rotated by 135°, detail) and corresponding to the stratigraphy of Fig. 10, unetched, polarised light. The metal appears in blue and the corrosion changes from yellow-orange (CP4) to dark-red (CP3), black (CP2) and orange (CP1). The area selected for elemental chemical distribution (Fig. 9) is marked by a red rectangle,

Fig. 9: SEM image, BSE-mode, and elemental chemical distribution of the selected area from Fig. 8. Method of examination: SEM/EDS, Laboratory of Analytical Chemistry, Empa..

Fig. 10: Stratigraphic representation of the sample taken from the sword in cross-section (dark field) using the MiCorr application. The characteristics of the strata are only accessible by clicking on the drawing that redirects you to the search tool by stratigraphy representation. This representation can be compared to Fig. 8, Credit HE-Arc CR.

▼ Synthesis of the binocular / cross-section examination of the corrosion structure

None.

▼ Conclusion

The sword blade is made of a hard, P-rich iron. It displays poor workmanship compared to other Celtic swords. The metal was first hot worked followed by a final cold working. The corrosion layer, typical of terrestrial context, has been partially removed by the conservation treatment. The possible use of air abrasive cleaning with glass beads and aluminium oxide, or the use of abrading tools, could explain the enrichment in Si and Al of the surface.

▼ References

References on object and sample

References object

1. Senn Bischofberger, M. (2005) Das Schmiedehandwerk im nordalpinen Raum von der Eisenzeit bis ins frühe Mittelalter. Internationale Archäologie, Naturwissenschaft und Technologie Bd. 5, (Rahden/Westf.), 30.

References sample

2. Senn Bischofberger, M. (2005) Das Schmiedehandwerk im nordalpinen Raum von der Eisenzeit bis ins frühe Mittelalter. Internationale Archäologie, Naturwissenschaft und Technologie Bd. 5, (Rahden/Westf.), 240-242.

References on analytic methods and interpretation

3. Swiss, A. J. and McDonnell, J.G. (2003) Evidence and interpretation of cold working in ferritic iron. International Conference, Archaeometallurgy in Europe 2003, Proceedings, vol. 1, Milan, 209-217.
4. ASTM E112-13: Standard Test Methods for Determining Average Grain Size.